Electrochemical CO₂ Reduction Catalytic Activity and Materials Characterization of Heterogeneous Zinc Carbonaceous Layers Derived from a Zinc(II) Molecular Catalyst

Francois Nkurunziza,^a Christine A. Phipps,^b Dillon T. Hofsommer,^b Matthew C. Mulvehill,^a Craig A. Grapperhaus,^{b*} and Joshua M. Spurgeon^{a*}

^a Conn Center for Renewable Energy Research, University of Louisville, Louisville, Kentucky 40292, USA.

^b Department of Chemistry, University of Louisville, 2320 South Brook Street, Louisville, Kentucky 40292, USA.

KEYWORDS

CO2 reduction, Zn(DMTH), molecular catalysis, heterogeneous catalysis, formic acid

ABSTRACT

Homogeneous molecular electrocatalysts have promise as a highly tailorable platform for designing active sites with high selectivity for target products. However, many such catalysts

face durability issues under applied potential, which can cause reductive or oxidative decomposition of the molecule. The resulting deposition of the metal center and possible ligand fragments on the electrode surface as a heterogeneous catalyst convolutes the measured electrochemical activity, leading to uncertainty regarding the role of the molecular catalyst. molecular Zn(DMTH) (DMTH Herein. the catalyst diacetyl-2-(4-methyl-3thiosemicarbazonate)-3-(2-pyridinehydrazonato), which has been reported for CO₂ reduction activity to formate, was investigated carefully to uncover the role of its reductive decomposition to form a heterogeneous zinc carbonaceous layer (HZCL) on the cathode. The deposited film appears to be primarily responsible for the CO₂ reduction activity to formate, with the current density and formate faradaic efficiency increasing over time as the layer develops. Interestingly, deposition of the HZCL under CO₂ bubbling led to a significantly more formate-selective catalyst layer than deposition of the HZCL under Ar bubbling. The morphological and chemical nature of the Zn(DMTH)-derived films were studied via several electrochemical and materials characterization techniques to provide insight on the catalyst layer and which aspects may contribute to the observed difference between HZCL film types.

INTRODUCTION

While the continuing development of carbon-free renewable energy sources is vital to slow the emission of greenhouse gases, another emerging key technology is the conversion of CO₂ to value-added chemicals and fuels.¹⁻⁵ Among the various feasible processes for CO₂ conversion, electrochemical reduction has critical advantages, including operation at room temperature and atmospheric pressure and a high product selectivity which can be tuned by the

choice of electrocatalyst, electrolyte, and the applied potential. Moreover, renewable electricity generated by solar and wind can be directly utilized in electrochemical CO₂ reduction (CO₂R), providing another energy storage outlet to ease the intermittent nature of these sources and avoid electricity curtailment while simultaneously enabling the carbon-negative synthesis of valuable products.⁵

Catalyzing electrochemical CO₂R remains a difficult task due to complex reaction pathways that can lead to a variety of products, in addition to the relative stability of the C=O bond.^{1, 3} These challenges have motivated the development of molecular electrocatalysts that decrease the CO₂R activation energy and improve the selectivity for target products. Redoxactive transition metal complexes in particular have attracted significant attention as their properties and activity can be tuned by ligand design.^{6, 7} A wide variety of transition metal complexes have been extensively investigated as inexpensive earth-abundant catalysts in electrochemical and solar fuels applications.⁸ Various complexes of non-noble metals such as Fe, Co, Mn, Ni, and Cu have demonstrated the ability to electrochemically reduce CO₂ to CO, HCOO⁻, and H₂ with promising selectivity. Fe-based complexes with porphyrin or porphyrin-like ligands have been shown to produce CO with > 90% faradaic efficiency (FE). Also, a number of Co-based complexes have been reported to electrochemically reduce CO₂ selectively to formate, including a compound with redox-active imino bipyridine ligands achieving 80% formate FE in acetonitrile and another compound with diphosphine ligands with pendant amines enabling 90% FE in dimethylformamide/water mixtures.^{9, 10} However, a critical challenge for these molecular electrocatalysts is their frequent instability under operating conditions. Reduction can decrease ligand stability due to the addition of electrons on the metal complex while oxidation can lead to ligand decomposition.^{6, 11}

Under electrocatalytic conditions, some of these molecular complexes degrade into other homogeneous or heterogeneous catalytic active species. 12, 13 Consequently, a comprehensive study of such fragile molecular catalysts must consider the resulting degradation or decomposition during electrochemical operation.^{6, 14} Qualitative analysis of the cyclic voltammogram (CV) serves as a primary indication of catalyst transformation, especially in cases where the decomposition involves heterogeneous species depositing or adsorbing on the surface of the electrode. CVs displaying irreproducibility over multiple scans, pre-catalytic waves, curve-crossing, and unexpected peaks during the reverse scan are major indications of catalyst degradation. Catalyst degradation can also be identified by film deposition on the electrode surface, which is common in molecular catalysis.^{6, 14-17} For instance, the molecular complex boron-capped tris(glyoximato) cobalt clathrochelate was found to act as a pre-catalyst that degrades under cathodic potentials to cobalt-containing nanoparticles adsorbed on the electrode surface. After rinsing the electrode surface and testing the adsorbed cobalt-containing nanoparticles in the absence of the homogeneous molecular cobalt complex, the result confirmed that the deposited cobalt species was more catalytically active for hydrogen evolution than the parent complex.¹⁸

Recently, our group has developed the ligand DMTH ((DMTH = diacetyl-2-(4-methyl-3-thiosemicarbazonate)-3-(2-pyridinehydrazonato)) in coordination with transition metals such as Ni, Pd, Cu, and Zn as molecular complex co-catalysts for the hydrogen evolution reaction (HER) and CO₂R.¹⁹⁻²¹ The advantage of Zn(DMTH), and its derivatives,²² is the ability to bind CO₂, including from low concentration sources such as air, thereby generating an activated form of CO₂ that can readily be reduced. Zn(DMTH) forms a bright orange solution in methanol that rapidly turns yellow when bubbled with CO₂. The orange color returns when the solution is

sparged with an inert gas, indicating the reversibility of the CO₂ binding.²⁰ In a previous HER study, it was observed that Zn(DMTH) degraded into an amorphous film that was weakly adsorbed on the electrode surface when subjected to prolonged electrolysis.¹⁹ A similar film deposition on the cathode was observed during electrolysis in methanol under active bubbling of CO₂.²⁰

To unravel the nature of the homogeneous vs. heterogeneous CO₂R activity of Zn(DMTH), we have investigated the electrocatalytic behavior of the degradation film in methanol in comparison with the pristine Zn(DMTH) solution in methanol. Two types of cathode heterogeneous zinc carbonaceous layer (HZCL) films were fabricated and tested: HZCL films deposited on glassy carbon from Zn(DMTH) under cathodic potentials in methanol while bubbling with either Ar (HZCL-Ar) or CO₂ (HZCL-CO₂). Interestingly, these two HZCLs had notably different CO₂R selectivity to formate, both of which were higher than either pristine homogeneous Zn(DMTH), a Zn foil, or ZnO nanoparticles (NPs) at the same amount of charge passed. The chemical and morphological nature of the deposited degradation HZCL film is thus crucial to its CO₂R activity, which is described herein by a variety of electrochemical and materials characterization techniques.

EXPERIMENTAL

Zn(DMTH) Synthesis. All solvents were obtained from commercial sources and used as received. Diacetyl-2-(4-methyl-3-thiosemicarbazone)-3-(2-pyridinehydrazone) (H₂DMTH) ligand was prepared by a previously reported method.²³ Zinc acetate dihydrate (0.225 g, 1.23 mmol) was added to (H₂DMTH) (0.245 g, 0.927 mmol) in 30 mL of ethanol, and the mixture

was refluxed under N_2 for ~ 16 h. The product was rinsed with cold ethanol and diethyl ether and the purity was confirmed by 1H nuclear magnetic resonance (NMR) spectroscopy.

Electrochemical Measurements. All electrochemical experiments were performed in an H-cell with a glass frit separating the anode and cathode chambers (Figure 1). The cell was cleaned by rinsing with acetone followed by DI water and dried in the oven prior to use. The working electrode was made from a glassy carbon plate (>99.99%, 4 mm thick, Alfa Aesar). The glassy carbon was silver-painted to a copper wire encased in a glass tube and sealed with Loctite EA9460 epoxy. The glassy carbon electrodes (GCEs) were cut into pieces with a projected geometric active area of 0.30 - 0.36 cm², which is roughly 4x greater than a typical glassy carbon rotating disk electrode. Prior to first use, the GCE was polished with an aqueous solution of alumina slurry, rinsed with DI water and methanol, and then dried in air. A Pt mesh and a Ag/AgCl (3 M KCl) were used as the counter and reference electrodes, respectively. For experiments producing an HZCL on the working electrode, the catholyte consisted of 1.0 mM Zn(DMTH) molecular catalyst in methanol solution containing 0.1 M tetrabutylammonium hexafluorophosphate (TBAPF6 or Bu4NPF6) salt and 10 mM acetic acid as a proton source. The anolyte consisted of 0.1 M TBAPF6 methanol solution. Either an Ar or CO2 input gas at a flowrate of 20 sccm using an MKS mass flow controller was saturated with methanol in an upstream bubbler before being introduced into the cell catholyte via a porous glass gas diffuser. The cell was constantly stirred to mitigate any species diffusion limitations near the electrode surfaces. A Biologic potentiostat (SP-200) was used for all electrochemical measurements. When synthesizing the Zn(DMTH)-derived films, the initial CV behavior at a scan rate of 100 mV s⁻¹ was recorded followed by a chronoamperometric (CA) measurement at -1.9 V vs Ag/AgCl until 50 C of charge was passed resulting in HZCL film deposition on the working electrode surface.

The HZCL-coated GCE was then gently rinsed in fresh methanol solution and dried in air for > 12 h. Subsequent experiments investigating the catalytic activity of the HZCLs themselves contained no Zn(DMTH) in the catholyte. Additional comparison experiments used working electrodes consisting of either a Zn foil (99.9% purity, Strem Chemicals) or ZnO NPs on a GCE. ZnO NP electrodes were prepared by dispersing 5 mg of Zn NPs (dry powder of 20 – 30 nm diameter particles, 99% purity, Thermo Scientific) in 10 mL of DI water, ultrasonicating for 30 min, drop-casting onto a blank GCE, and then drying in air at room temperature for several hours. CV and CA measurements were conducted on each electrode type to characterize the electrochemical behavior. After each CA measurement, a 2.0 mL aliquot of the catholyte was collected for product analysis.

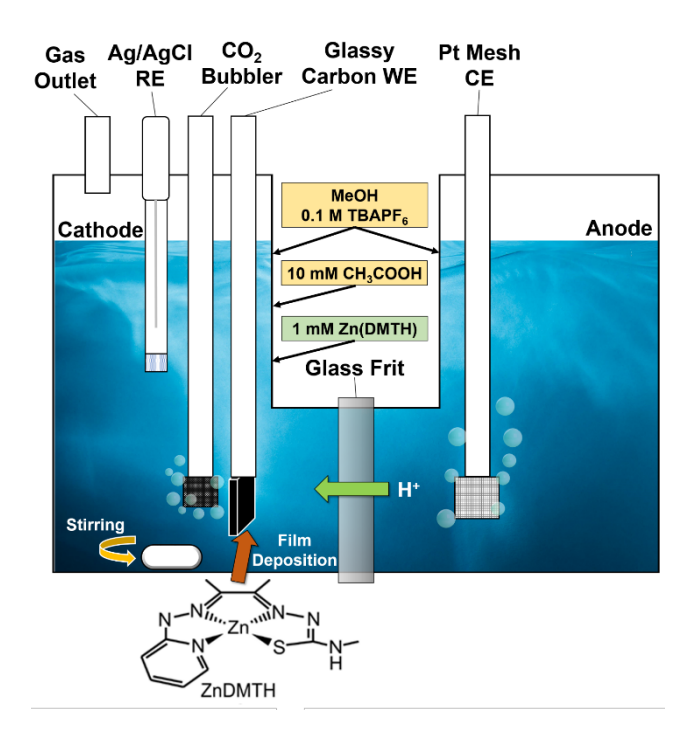


Figure 1. Schematic of the H-cell used for electrochemical experiments with a glassy carbon working electrode (WE), Pt mesh counter electrode (CE), and Ag/AgCl reference electrode (RE).

During HZCL film deposition experiments only, 1.0 mM Zn(DMTH) was present in the catholyte.

Product Quantification. The CO₂R liquid products were analyzed by nuclear magnetic resonance (NMR) spectroscopy (Agilent V NMRS 700 MHz). After each CA electrolysis experiment, a 600 μL aliquot of the catholyte solution was sampled and mixed with 200 μL of d6-DMSO (99.9%, Cambridge Isotope Laboratories) and prepared to a final concentration of 3 mM DMF as an internal standard.²⁴ The chemical shifts were referenced to DMSO at 2.5 ppm. Integration of the formate peak (chemical shift at ~8.4 ppm) was quantified using the internal standard DMF peak and a calibration curve. For real-time gas phase product analysis, the outlet of the cathode compartment was connected to the inlet for a gas chromatograph (GC, SRI 8610). The GC system used an automatic valve injection (1 mL sample) and a thermal conductivity detector (TCD) and flame ionization detector (FID). Ultra-high purity nitrogen (99.99%, Specialty Gases) was used as the carrier gas for all experiments and was chosen to enable accurate hydrogen quantification. Faradaic efficiency (FE) was calculated by dividing the charge required to yield the measured product concentration by the total charge passed during electrolysis as determined by the potentiostat.

Materials Characterization. The electrode HZCL films were characterized with scanning electron microscopy (SEM) of the morphology and energy-dispersive x-ray spectroscopy (EDS) elemental mapping and quantification using a TESCAN Vega3 microscope with a built-in EDS detector. Surface analysis was performed using x-ray photoelectron spectroscopy (XPS) with a VG Scientific Multilab 3000 custom-built ultra-high vacuum system with Al-Kα radiation.

Fourier transform infrared (FTIR) spectroscopy data was measured on a Thermo Scientific Nicolet iS20 spectrometer. X-ray diffraction (XRD) data were collected using a Bruker Discovery D8-HR x-ray diffractometer with a Cu-Kα source.

RESULTS AND DISCUSSION

Electrochemical Characterization. Under potentiostatic operation in the methanol electrolyte in the presence of Zn(DMTH), the gradual formation of an HZCL at the GCE surface was visible by the naked eye. Figure 2 shows representative images of the pristine electrode surface and a typical film after passing 50 C. Although the HZCL deposited across the entire electrode, there were clear regions of inhomogeneity. The inhomogeneity and bare spots in the HZCL films were qualitatively associated with the observation of bubble generation during electrolysis.

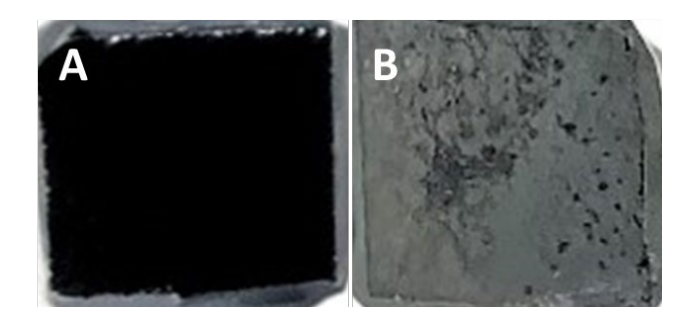


Figure 2. Optical photographs of the surface of (A) a pristine GCE before HZCL deposition and (B) an HZCL film deposited on a GCE in the presence of Zn(DMTH) in methanol. The grey edges are epoxy.

The electrochemical CV behavior in the presence of Zn(DMTH) was measured as shown in Figure 3. Voltammograms with a GCE in a 10 mM acetic acid methanol solution of Zn(DMTH) under either Ar or CO₂ bubbling both exhibited an irreversible prewave of oxidative current between -0.7 to -1.0 V vs Ag/AgCl prior to the main reductive current catalytic wave at more cathodic potentials. The irreversible peak was indicative of an electrochemical process other than CO₂R and was attributed to an oxidative decomposition pathway. Notably, a blank GCE working electrode in the same catholyte mixture without Zn(DMTH) displayed a similar oxidative peak in this potential range, but the peak was not present in the absence of the 10 mM acetic acid component (Figure S1). Thus, this peak at ~ -0.9 V vs Ag/AgCl was attributed to oxidation of the acetate. Oxidation of the Zn(DMTH) was not the main route for the transformation or decomposition of the molecular catalyst, as potentiostatic operation at -1.9 V vs Ag/AgCl while passing reductive current led to the gradual formation of the visible surface HZCL films as shown in Figure 2. Thus, a reductive mechanism was responsible for the Zn(DMTH) breakdown and subsequent adsorption of the heterogeneous films investigated in this study. Both types of HZCL films, whether deposited under Ar (HZCL-Ar) or CO₂ (HZCL-CO₂), displayed oxidative current at potentials positive of -1.0 V vs Ag/AgCl in the absence of Zn(DMTH) (Figure 3b). To prevent possible oxidative decomposition of the HZCL, only reductive current was passed in subsequent experiments and prior to materials characterization. The corresponding electrochemical behavior for a Zn foil electrode and a GCE decorated with ZnO NPs is shown in Figure S2 for comparison.

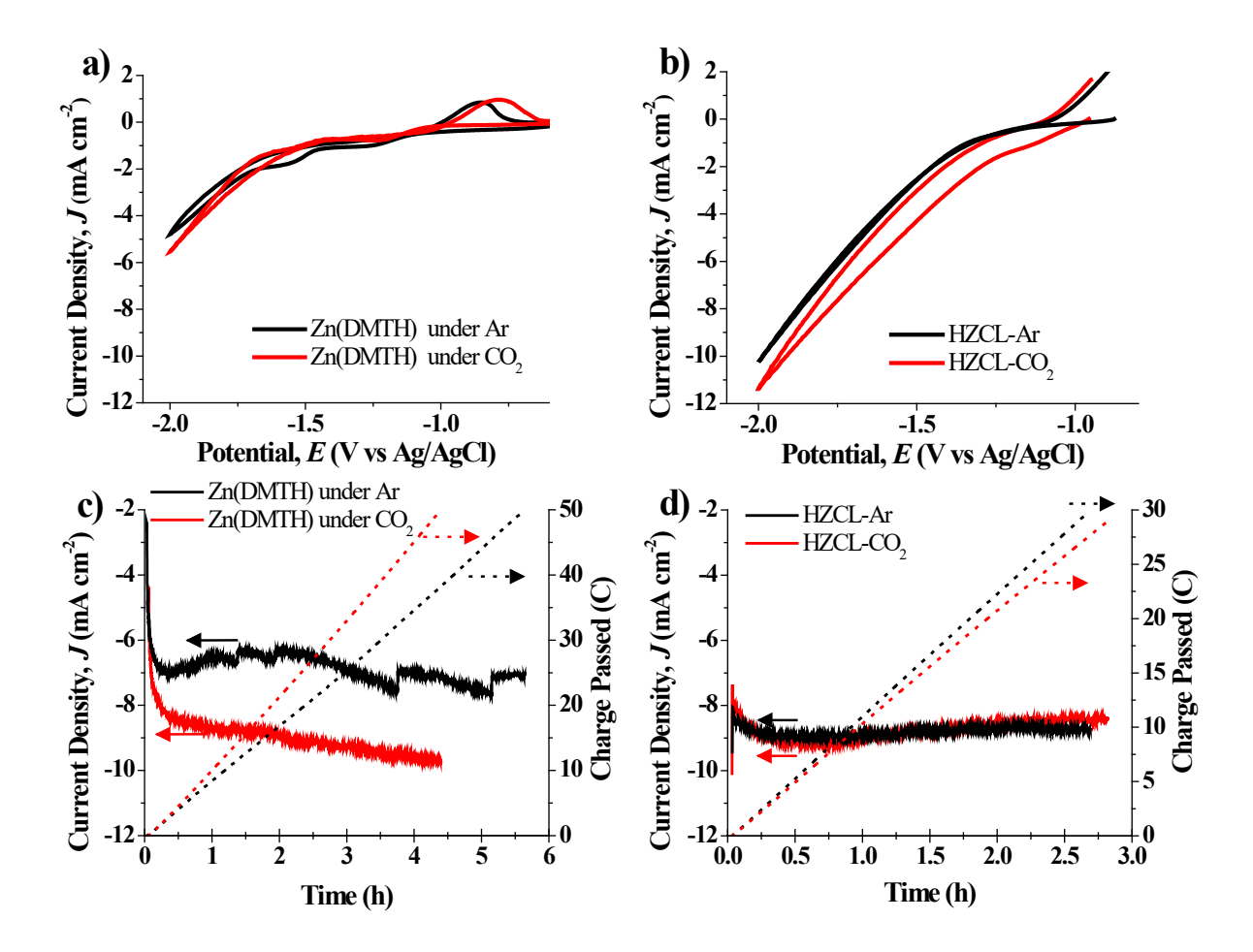


Figure 3. Electrochemical behavior in the presence of Zn(DMTH) bubbled under Ar or CO₂ and the corresponding behavior of deposited HZCL films. (a-b) Initial current density vs. potential behavior and (c-d) current density and cumulative charge passed at -1.9 V vs Ag/AgCl over time in 0.1 M TBAPF₆ and 10 mM acetic acid in methanol solution. (a, c) The behavior of a glassy carbon working electrode bubbled under either Ar or CO₂ with 1.0 mM dissolved Zn(DMTH) catalyst in the catholyte. (b, d) The behavior of the subsequent HZCL resulting from Zn(DMTH) degradation under Ar (HZCL-Ar) or CO₂ (HZCL-CO₂) deposited on a GCE and measured under CO₂ bubbling in the absence of Zn(DMTH) catalyst.

The catalytic activity of Zn(DMTH) and the corresponding deposited HZCL films was investigated via electrolysis with chronoamperometric measurements at -1.9 V vs Ag/AgCl. The current density behavior of an initially blank GCE in 1.0 mM Zn(DMTH) while bubbling either Ar or CO₂ until the passage of 50 C is shown in Figure 3c. Notably, in both cases, a significant reductive current increase occurred in the first 30 min of electrolysis and thereafter a much more gradual increase in the current was observed. The sharp increase in current in the beginning is consistent with the beginning phase of Zn(DMTH) decomposition and HZCL film formation. Adsorption of the Zn-containing film material puts it in intimate contact with the GCE as a heterogeneous catalyst, eliminating the mass transfer limitations and lessening the chargetransfer limitations associated with Zn in the homogeneous catalyst state. Indeed, the resulting HZCLs displayed higher current density in the absence of Zn(DMTH) (Figure 3b) than the initial blank GCE in the presence of Zn(DMTH) (Figure 3a). Thus, the rapid current increase over the first 30 min can be attributed to HZCL formation and increasing GCE surface coverage (Figure 3c). Once the surface was fully coated, any further increase in current density would be limited to a modest enhancement to the electrochemically active surface area as the film grew thicker. The chronoamperometric behavior of the resulting HZCL films in the absence of Zn(DMTH) supports this interpretation, with both HZCL-Ar and HZCL-CO₂ displaying fairly steady current density vs time without Zn(DMTH) to adsorb and further grow the films (Figure 3d).

Under active bubbling of CO₂, the liquid product selectivity of various electrodes was determined by quantifying the FE of formate after chronoamperometric electrolysis (Table 1). For an initially blank GCE in 1.0 mM Zn(DMTH), the CO₂R selectivity was measured after the passage of 30, 60, and 100 C, resulting in formate FEs of 9.2, 22.8, and 32.6%, respectively. The corresponding HZCL made under CO₂ (HZCL-CO₂) resulted in 36.7% formate FE after passing

30 C in the absence of Zn(DMTH). The HZCL-CO₂ activity was thus 4x higher than a blank GCE in Zn(DMTH) after passing the same amount of charge, indicating that CO₂R activity for formate could be primarily attributed to the heterogeneous film layer. Moreover, the gradual increase in formate FE for an initially blank GCE in Zn(DMTH) was attributed to the activity of HZCL-CO₂ developed in-situ, with the FE value after 100 C approaching the value for the predeposited HZCL-CO₂ (Table 1).

Table 1. Measured CO₂R faradaic efficiencies (FE) for formate for chronoamperometric experiments at -1.9 V vs Ag/AgCl in 0.1 M TBAPF₆ and 10 mM acetic acid in methanol. The cases with Zn(DMTH) had the compound present in the catholyte at 1.0 mM and started with a pristine glassy carbon working electrode.

Catalyst	Charge Passed (C)	HCOO- FE (%)
Zn(DMTH)	30	9.2
Zn(DMTH)	60	22.8
Zn(DMTH)	100	32.6
HZCL-Ar	30	16.8
HZCL-CO ₂	30	36.7
Zn Foil	30	15.3
ZnO NPs	30	12.2

Further insight can be gained by analyzing the gaseous products during electrolysis with an initially blank GCE in Zn(DMTH) under CO₂ bubbling (Figure 4). The majority of the gaseous product was CO with a measured FE of 55%, decreasing to \sim 45% by the end of the electrolysis. The H₂ FE increased from an initial value of 7% to \sim 25% after the passage of 50 C. Thus, the total FE for gaseous products was fairly steady at 60 – 70%. Over this same time

period, the liquid product formate FE increased from the low single digits and approached 20% (Table 1). The balance of charge passed is assumed to be attributable to the reductive decomposition of Zn(DMTH) and adsorption of the HZCL. Film formation thus represented a greater fraction of the charge passed at short times than it did at longer times.

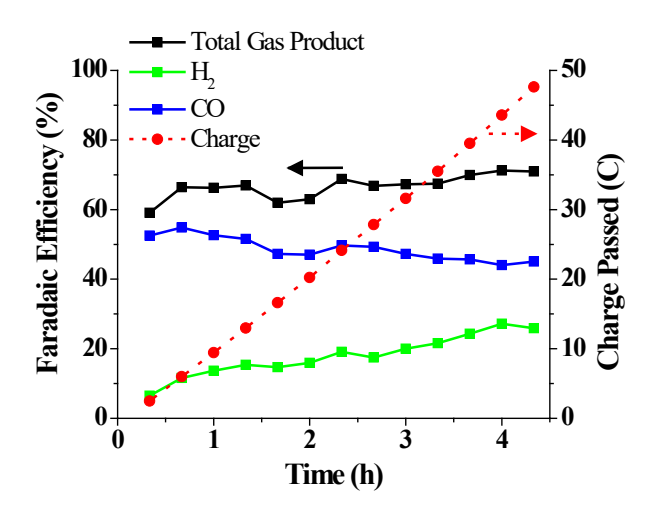


Figure 4. Gaseous product faradaic efficiencies and cumulative charge passed vs time at -1.9 V vs Ag/AgCl for a pristine GCE in 1.0 mM Zn(DMTH) in 0.1 M TBAPF₆ and 10 mM acetic acid in methanol solution bubbled under CO₂.

The HZCL films generated under a constant reducing potential in Zn(DMTH), though not strongly bound to the GCE surface, were not soluble in methanol. The catalytic activity of the isolated HZCLs were thus tested by rinsing the GCE surface with methanol, air drying, introducing the HZCL/GCE to fresh methanol electrolyte without Zn(DMTH), and evaluating the electrochemical behavior under CO₂. Interestingly, HZCL films deposited under Ar (HZCL-Ar) were observed to have distinctly lower formate FE than HZCLs deposited under CO₂ (HZCL-CO₂). After 30 C of CO₂R, HZCL-Ar exhibited an average of 16.8% formate FE, less

than half the 36.7% average formate FE measured for HZCL-CO₂ (Table 1). This finding was strongly reproducible, with narrow error bars determined over 6 redundant experiments (Figure 5a). For comparison, a Zn foil electrode and a GCE decorated with ZnO NPs were also measured under the same conditions (Figure S2), leading to formate FEs of 15.3 and 12.2%, respectively (Table 1, Figure 5a). Because of its similar current density behavior and formate FE to Zn foil, the activity and selectivity of HZCL-Ar could be attributable to the dominance of elemental Zn in the film. However, the enhanced CO₂R activity for formate for HZCL-CO₂ relative to Zn Foil indicates that some aspect of the morphology and/or composition of this layer has improved the formate synthesis route relative to an elemental Zn surface alone.

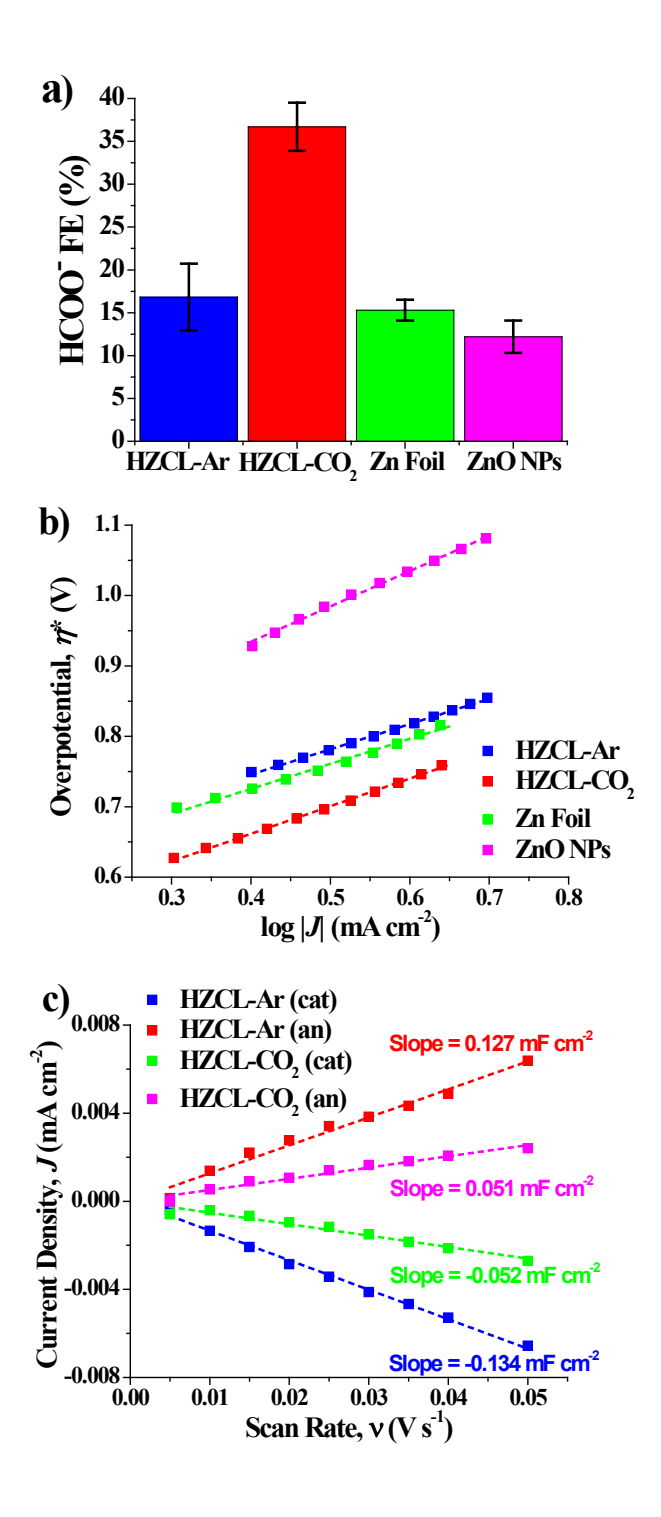


Figure 5. CO₂R catalysis data for the HZCL films compared to Zn-based electrodes. (a) The CO₂R faradaic efficiency to formate after passing 30 C at -1.9 V vs Ag/AgCl in 0.1 M TBAPF₆ and 10 mM acetic acid in methanol in the absence of Zn(DMTH). (b) Tafel data for electrodes

using the log of the current density, J, vs an estimated overpotential, η^* . The working electrodes were HZCLs on a GCE deposited under active bubbling of either Ar (HZCL-Ar) or CO₂ (HZCL-CO₂) or comparison standards of a Zn Foil or ZnO nanoparticles deposited on a GCE. (c) Cathodic (cat) and anodic (an) charging current densities from double-layer capacitance measurements on HZCL-Ar and HZCL-CO₂.

The current density vs voltage behavior of HZCL-Ar, HZCL-CO₂, Zn foil, and ZnO NPs were converted into Tafel data of the log of the current density, J, vs an estimated overpotential, η^* (Figure 5b). The overpotential is emphasized as an estimate due to uncertainties in some parameter values when operating in methanol solvent, and the method of calculating η^* is described in the SI. From the resulting Tafel behavior, some qualitative comparisons can be made between the electrodes regarding the reaction kinetics. The ZnO NPs had by far the highest overpotentials and also a notably higher Tafel slope than the other three electrode types. This implies more kinetically inhibited CO₂R on ZnO in this system and also suggests the heterogeneous film behavior is not dominated by ZnO active sites. On the other hand, the HZCL-Ar and Zn foil electrodes exhibited very similar Tafel data, providing further electrochemical evidence to suggest the HZCL-Ar catalytic activity is primarily influenced by elemental Zn. The HZCL-CO₂, while having a comparable Tafel slope to HZCL-Ar, had notably lower overpotential. Consequently, HZCL-CO₂ had an exchange current density 2.5x higher than that of HZCL-Ar. Because Tafel slope is understood to be reflective of the electrocatalyst mechanism, a greater exchange current density at a comparable slope is generally indicative of a higher density of the active catalyst sites per geometric area.²⁵

Further electrochemical characterization was conducted to estimate the relative ratio of the electrochemically active surface area (ECSA) between HZCL-Ar and HZCL-CO₂. ECSA can be estimated by measuring non-faradaic capacitive current associated with double-layer charging from the scan-rate dependence of CVs and comparing this to the capacitance of a flat surface of the same material. Because of the uncertain nature of the heterogeneous Zn(DMTH)-derived films, no equivalent flat surface capacitance value is readily available, but the measured double-layer capacitance of the two HZCL types can be compared to gauge the difference in ECSA. A reliable potential window for purely non-faradaic current behavior was difficult to achieve in the methanol electrolyte, so double-layer capacitance measurements were instead performed by transferring the HZCL/GCEs to acetonitrile solvent for analysis. The aprotic nature and wide solvent window of acetonitrile enabled reproducible scan-rate dependent measurements for HZCL-Ar and HZCL-CO₂ in regions of primarily non-faradaic capacitive current (Figure S3).

The scan-rate dependence of the charging current density for the cathodic and anodic sweeps are shown in Figure 5c. HZCL-Ar and HZCL-CO₂ had average double-layer capacitance values of 0.131 and 0.052 mF cm⁻², respectively. Assuming a similar intrinsic capacitance for these film materials, this result indicates that HZCL-Ar had ~ 2.5x higher ECSA than HZCL-CO₂. The lower ECSA for HZCL-CO₂ is somewhat surprising considering its enhanced activity and selectivity relative to HZCL-Ar, as reflected by the formate FE and Tafel data, which indicates sluggish kinetics at much of the HZCL-Ar surface area. During film deposition from electrolysis in the presence of Zn(DMTH), bubbling CO₂ led to appreciable faradaic current for CO₂R (Table 1, Figure 4). Thus, after passing 50 C, a smaller fraction of this charge was directed to the reductive decomposition of Zn(DMTH) and adsorption of HZCL-CO₂ as compared to passing 50 C under Ar to make HZCL-Ar. The HZCL-Ar layers were observably thicker as a

result. We therefore speculate that the higher measured ECSA of HZCL-Ar may be attributable to the porous permeable nature of the film allowing a greater depth of this thicker HZCL to be electrochemically accessible.

Materials Characterization of the HZCL Films. Beyond the electrochemical properties of the heterogeneous Zn(DMTH)-derived films, insight into their morphological and chemical composition was obtained by characterization through a variety of microscopy, spectroscopy, and x-ray diffractometry methods. Although some macroscopic variation in the HZCL films was observable across the electrode area (Figure 2), the majority of the HZCL surface morphology was characterized by SEM with some representative images shown in Figure 6 and Figure S4. Both types of heterogeneous films displayed appreciable microscopic surface roughness, but the HZCL-CO₂ surfaces had visibly greater levels of protrusions and a fold-like surface morphology. These fold-like features also showed micron-scale roughness at a greater level than the corresponding HZCL-Ar surface.

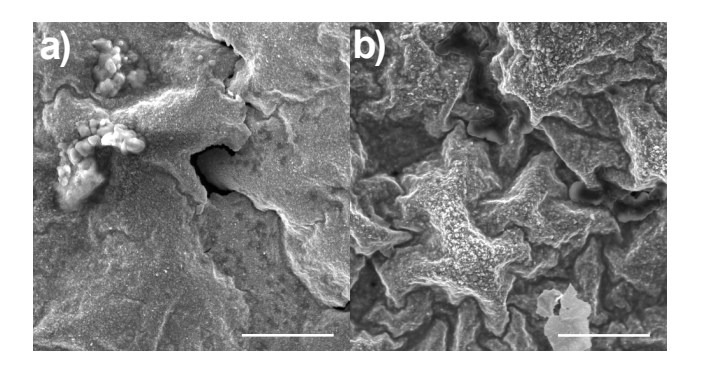


Figure 6. Representative SEM images of (a) HZCL-Ar and (b) HZCL-CO₂. The scale bar in each image is 50 μm.

Quantitative EDS characterization across many spots on several different electrodes was used to gather data on the elemental composition between HZCL-Ar and HZCL-CO₂ (Table 2). The most notable difference between the film types was that HZCL-Ar was consistently measured to have much higher percentages of Zn in the layer. HZCL-Ar had an average Zn composition of 55.6 at%, approximately double the 27.5 at% for HZCL-CO₂. This compositional difference was balanced by a much higher carbon atomic percentage consistently measured in the HZCL-CO₂. While EDS only provides bulk elemental information and does not reveal the bonding environment, the higher fraction of Zn in HZCL-Ar indicates that a greater amount of metal from the Zn(DMTH) deposited on the GCE surface in this case. The higher measured carbon percentage in the HZCL-CO₂ might be attributable to more of the Zn(DMTH) ligand structures being incorporated in the film, but could conceivably also come from higher sampling of the underlying glassy carbon substrate in thin regions of the HZCL. Very low sulfur percentages, generally within the error of the measurement, were detected in either film, suggesting that this region of the DMTH ligands decomposed and was not appreciably incorporated into the HZCL. In addition, there were consistent measurements of fluorine and phosphorus at 0.5 - 5 at%, which was attributed to permeation of the TBAPF₆ supporting electrolyte into the film during deposition.

Table 2. Elemental atomic percentage composition as measured by EDS surveying of cathode HZCL films deposited under active bubbling of either Ar or CO₂. The atomic percent is the average and the error is the standard deviation from twelve different measurements.

	HZCL-Ar		HZCL-CO ₂	
Element	Atomic %	Error (%)	Atomic %	Error (%)
C	30.9	± 5.6	56.0	± 9.4
O	10.7	± 4.1	9.3	± 4.6
F	2.0	± 0.7	4.8	± 2.0
P	0.6	± 0.3	2.3	± 0.8
S	0.1	± 0.1	0.1	± 0.2
Zn	55.6	± 5.7	27.5	± 10.0

The chemical state of the surface of the HZCL films was analyzed with XPS and compared to the spectra for pristine Zn(DMTH) powder (Figure 7). The pristine Zn(DMTH) exhibited clear binding energy peaks for the N 1s and S 2p3/2 orbitals as expected considering the nitrogen and sulfur bonds present in the DMTH ligand (Figure 1). However, after electrolytic operation in Zn(DMTH) to form the heterogeneous films, neither HZCL-Ar nor HZCL-CO2 displayed any appreciable trace of nitrogen or sulfur. Thus, these parts of the ligand structure are assumed to have decomposed or otherwise were not adsorbed during HZCL deposition. Since the Zn(DMTH) metal center is only bonded to N and S atoms, the absence of these peaks suggests that the Zn has been fully removed from the ligand structure during film formation. In contrast, both HZCL types exhibited strong peaks for the Zn 2p3/2 orbital. However, while pristine Zn(DMTH) had the Zn 2p3/2 peak at 1021.4 eV, the corresponding peaks for the HZCL films where shifted to a slightly higher binding energy at 1021.7 eV. From the NIST database, this binding energy value could be consistent with either ZnO or elemental Zn. However, because a shift to higher binding energy generally indicates an increase in the oxidation state, these peaks

likely indicate the presence of a native Zn oxide layer formed during exposure to ambient air. The spectrum for each surface was normalized to the C 1s peak (Figure S5). The higher measured intensity for the Zn 2p3/2 peak for HZCL-Ar relative to HZCL-CO₂ thus indicates a greater Zn concentration at the surface for HZCL-Ar, which is in agreement with EDS measurements (Table 2). Similarly, HZCL-Ar displayed a higher intensity for the O 1s peak than HZCL-CO₂, consistent with a greater surface oxygen content that would be expected for Zn with a native oxide surface.

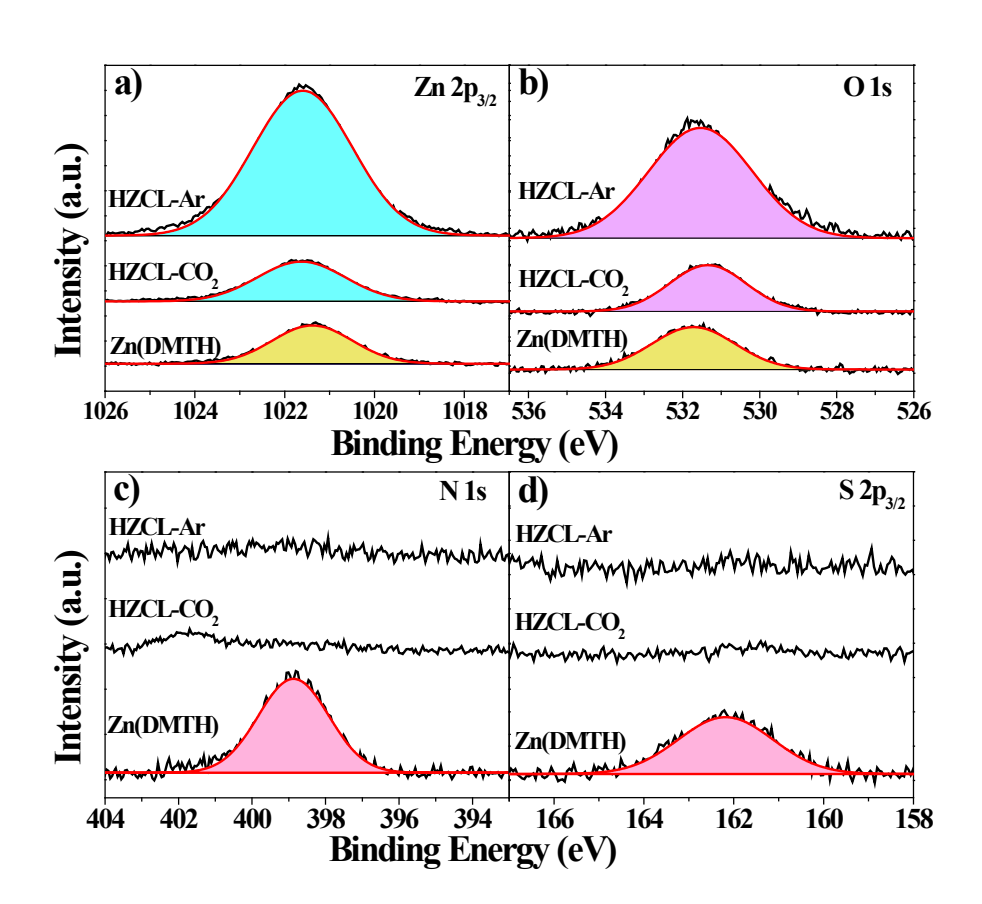


Figure 7. XPS spectra of pristine Zn(DMTH) powder and HZCL films on glassy carbon deposited under active bubbling of either Ar (HZCL-Ar) or CO₂ (HZCL-CO₂) for the (a) Zn 2p_{3/2} (b) O 1s, (c) N 1s, and (d) S 2p_{3/2} regions.

The bonding environment within the HZCLs was further probed using FTIR spectroscopy. Figure 8 shows the HZCL-Ar and HZCL-CO₂ spectra in comparison to the blank GCE, pristine Zn(DMTH), and a dry powder of the supporting electrolyte TBAPF₆. The transmittance data in Figure 8 was normalized to the highest peak intensity in each spectrum for ease of visual comparison. FTIR data prior to normalization is shown in Figure S6. While the FTIR spectrum for the blank glassy carbon was relatively featureless, the spectrum for the pristine Zn(DMTH) had many peak features due to the many different modes of vibration and stretching in the various bond types in the structure of the DMTH ligand. Notably, very few such peaks were observable at a significant intensity in either the HZCL-Ar or HZCL-CO₂, suggesting that little of the DMTH ligand structure remained intact within the heterogeneous films. The most prominent peak for the HZCLs was measured at 829 cm⁻¹, with lesser peaks at 556, 878, and 1474 cm⁻¹. The FTIR spectrum for an isolated sample of the TBAPF₆ supporting electrolyte salt displayed its most prominent features at the same wavenumbers. Each of the HZCL films was rinsed prior to FTIR measurement, which should remove most residual TBAPF6 from the surface. Thus, the observation of prominent FTIR peaks attributable to TBAPF6 indicates that an appreciable amount of the supporting electrolyte salt was incorporated into the HZCL itself. The FTIR data is thus consistent with the EDS measurements which found 0.6 – 2.3 at% P and 2.0 – 4.8 at% F (Table 2).

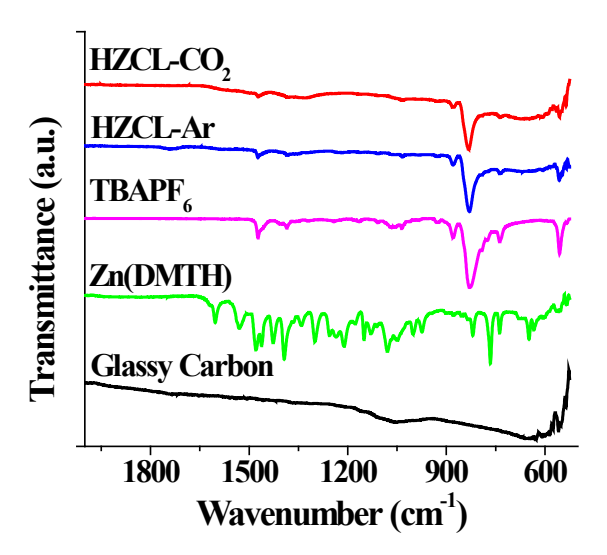


Figure 8. FTIR spectra of a blank glassy carbon electrode, pristine Zn(DMTH) powder, TBAPF₆ salt, and HZCL films on glassy carbon deposited under active bubbling of either Ar (HZCL-Ar) or CO₂ (HZCL-CO₂). The transmittance of each spectrum has been normalized to itself and offset for clarity.

Finally, the crystal structures of the heterogeneous films were investigated by mechanically removing the HZCLs from the GCE substrates and analyzing the film residue by powder XRD. Figure 9 shows diffraction data for HZCL-Ar, HZCL-CO₂, and pristine Zn(DMTH) powder. Zn(DMTH) powder did not exhibit any strong diffraction peaks. Both HZCL-Ar and HZCL-CO₂, in contrast, displayed a number of diffraction peaks that were indexed to the main crystal planes of elemental Zn. The corresponding peaks for ZnO were not observed, which indicates that the bulk of the Zn in the film was present in the elemental form.

The ZnO interpreted from the XPS data (Figure 7) was thus attributed primarily to a surface layer native oxide. The XRD diffractogram further supports the interpretation of the electrochemical data (Figure 5b), in which the catalytic behavior of the HZCLs much more closely resembles the activity of the Zn foil than the ZnO NPs. The Zn native oxide layer is assumed to electrochemically reduce at CO₂R reaction conditions, leaving elemental Zn sites to influence the catalytic activity. Notably, there was another peak observed at 28.0° that could not be indexed to Zn and did not appear in the diffraction data for Zn(DMTH). The nature of this peak remains uncertain, but we speculate that it could be related to the incorporation of the TBAPF₆ noted above.

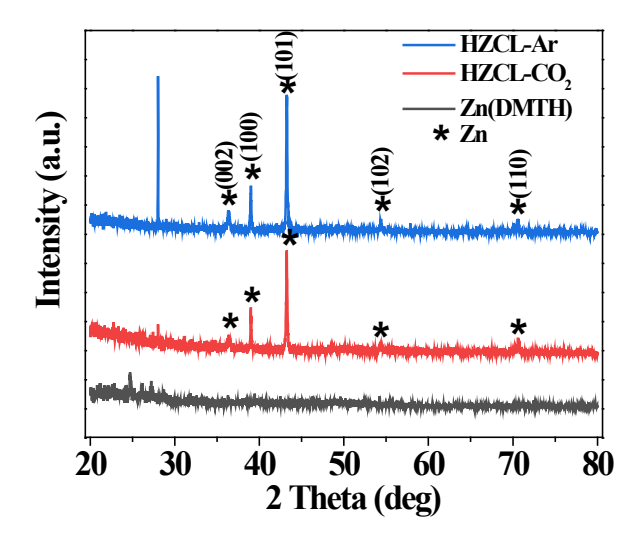


Figure 9. XRD data of pristine Zn(DMTH) powder and powders of HZCL films removed from the glassy carbon substrate that had been deposited under active bubbling of either Ar (HZCL-Ar) or CO₂ (HZCL-CO₂).

Taken altogether, the electrochemical and materials characterization data indicates that electrolysis at reductive conditions in methanol in the presence of Zn(DMTH) leads to a reductive decomposition of the N and S bonds to the Zn metal center and deposition of elemental Zn at the cathode in a film which contains carbonaceous material and also incorporates appreciable amounts of the TBAPF₆ supporting electrolyte species. Thus, previous reports of Zn(DMTH) molecular catalyst activity for CO₂R was probably attributable primarily to the activity of this HZCL film.²⁰ When this layer was deposited under Ar bubbling, more of the charge passed contributed to the reductive decomposition of Zn(DMTH) and film formation, leading to a thicker deposit with a greater fraction of Zn as evidenced by EDS and XPS. The HZCL-Ar thus displayed electrochemical activity and CO₂R selectivity very similar to a pure Zn foil (Figure 5). For HZCLs deposited under CO₂ bubbling, however, a large fraction of the charge was directed to CO₂R, leading to thinner deposits with less Zn (Table 2) and improved CO₂R activity and formate selectivity (Figure 5).

Since there was no measurable trace of the DMTH ligand in these heterogeneous films, the enhanced electrocatalysis for HZCL-CO₂ is probably attributable to morphological differences in the Zn deposit. Tafel data exchange current density values indicate a higher density of the active sites for HZCL-CO₂ compared to HZCL-Ar, despite higher measured ECSA for the thicker HZCL-Ar. SEM images did show more microscale surface roughness for the HZCL-CO₂ (Figure 6). Smaller Zn features in the HZCL-CO₂ may thus be responsible for the improved catalytic activity and formate selectivity. This explanation is supported by the CO₂ reduction literature, such as a report that Zn nanoparticles deliberately fabricated by electrochemical CO₂ reduction at an annealed Zn deposit led to major improvements in CO₂R formate FE in aqueous media without significantly changing the total current density.²⁸ The

enhanced formate selectivity was attributed to catalytically active facets of the nanocrystalline Zn surface. The improved CO₂R activity for formate production for Zn(DMTH)-derived films deposited during CO₂ reduction is thus likely attributable to the rougher Zn microstructure that results from the variation in deposition conditions.

CONCLUSIONS

Zn(DMTH), which has been reported as a molecular catalyst for the electrochemical conversion of CO₂ to formate in methanol, was studied to unravel the role played by the heterogeneous layer that deposits on the cathode during electrolysis. The CO₂R formate FE for a blank GCE in Zn(DMTH) increased over time as the HZCL developed, eventually approaching the formate FE value for the pre-deposited HZCL film measured in the absence of Zn(DMTH). Thus, the CO₂R activity can be primarily attributed to the heterogeneous catalyst layer rather than the homogeneous catalyst. Moreover, the HZCL deposited under CO2 bubbling was found to have more than twice the formate FE of a film deposited under Ar bubbling. XPS and FTIR indicated that little to no DMTH ligand was incorporated in the HZCL, while XRD showed that the films contained crystalline Zn deposits. EDS and XPS both indicated a higher Zn composition in the HZCL films deposited under Ar, which can account for these layers having similar electrochemical activity to Zn foil electrodes. SEM displayed a fold-like surface with a roughened microstructure for HZCL films deposited under CO2, and this microstructure was deemed to be the likely source of enhanced formate activity for the heterogeneous layer made under CO2. This study shows the importance of considering molecular breakdown and heterogeneous changes to the electrode surface when investigating the efficacy of molecular

catalysts and further highlights how subtle changes in deposition conditions can significantly

alter the electrochemical dynamic between the electrode, interface layer, and the homogeneous

molecular species.

ASSOCIATED CONTENT

Supporting Information. The following files are available free of charge.

Faradaic efficiency calculation; Tafel data calculation; blank glassy carbon electrochemical data;

Zn foil and ZnO NPs electrochemical data; double-layer capacitance measurements; HZCL SEM

images; XPS spectra for C 1s; FTIR without peak normalization (PDF)

AUTHOR INFORMATION

Corresponding Author

*E-mail: joshua.spurgeon@louisville.edu

Author Contributions

C.A.P. synthesized the Zn(DMTH) molecular catalyst. M.C.M. performed SEM and EDS

characterization. F.N. performed all other experiments and characterization measurements and

wrote much of the manuscript. C.A.G. and J.M.S conceived the project, supervised experimental

studies, and contributed to writing the manuscript. All authors have given approval to the final

version of the manuscript.

Funding Sources

28

This research was supported by the National Science Foundation (CHE-1955268).

Notes

The authors declare no competing financial interest.

ACKNOWLEDGMENTS

This material is based upon work supported by the U.S. National Science Foundation under Award Number CHE-1955268. The authors also acknowledge support from the Conn Center for Renewable Energy Research at the University of Louisville.

REFERENCES

- 1. Peter, S. C., Reduction of CO₂ to Chemicals and Fuels: A Solution to Global Warming and Energy Crisis. *ACS Energy Lett.* **2018**, *3*, 1557-1561, DOI 10.1021/acsenergylett.8b00878.
- 2. Zhang, X. L.; Guo, S. X.; Gandionco, K. A.; Bond, A. M.; Zhang, J., Electrocatalytic carbon dioxide reduction: from fundamental principles to catalyst design. *Mater. Today Adv.* **2020,** *7*, 100074, DOI 10.1016/j.mtadv.2020.100074.
- 3. Abdinejad, M.; Hossain, M. N.; Kraatz, H. B., Homogeneous and heterogeneous molecular catalysts for electrochemical reduction of carbon dioxide. *RSC Adv.* **2020**, *10*, 38013-38023, DOI 10.1039/d0ra07973a.
- 4. Kumar, B.; Brian, J. P.; Atla, V.; Kumari, S.; Bertram, K. A.; White, R. T.; Spurgeon, J., New trends in the development of heterogeneous catalysts for electrochemical CO₂ reduction. *Catal. Today* **2016**, *270*, 19-30, DOI 10.1016/j.cattod.2016.02.006.
- 5. Zhang, S.; Fan, Q.; Xia, R.; Meyer, T. J., CO₂ Reduction: From Homogeneous to Heterogeneous Electrocatalysis. *Acc. Chem. Res.* **2020**, *53*, 255-264, DOI 10.1021/acs.accounts.9b00496.

- 6. Lee, K. J.; McCarthy, B. D.; Dempsey, J. L., On decomposition, degradation, and voltammetric deviation: the electrochemist's field guide to identifying precatalyst transformation. *Chem. Soc. Rev.* **2019**, *48*, 2927-2945, DOI 10.1039/c8cs00851e.
- 7. Liu, D. C.; Zhong, D. C.; Lu, T. B., Non-noble metal-based molecular complexes for CO₂ reduction: From the ligand design perspective. *Energychem* **2020**, *2*, DOI 10.1016/j.enchem.2020.100034.
- 8. Boutin, E.; Merakeb, L.; Ma, B.; Boudy, B.; Wang, M.; Bonin, J.; Anxolabehere-Mallart, E.; Robert, M., Molecular catalysis of CO₂ reduction: recent advances and perspectives in electrochemical and light-driven processes with selected Fe, Ni and Co aza macrocyclic and polypyridine complexes. *Chem. Soc. Rev.* **2020**, *49*, 5772-5809, DOI 10.1039/d0cs00218f.
- 9. Liu, F. W.; Bi, J. J.; Sun, Y. S.; Luo, S. P.; Kang, P., Cobalt Complex with Redox-Active Imino Bipyridyl Ligand for Electrocatalytic Reduction of Carbon Dioxide to Formate. *Chemsuschem* **2018**, *11*, 1656-1663, DOI 10.1002/cssc.201800136.
- 10. Roy, S.; Sharma, B.; Peaut, J.; Simon, P.; Fontecave, M.; Tran, P. D.; Derat, E.; Artero, V., Molecular Cobalt Complexes with Pendant Amines for Selective Electrocatalytic Reduction of Carbon Dioxide to Formic Acid. *J. Am. Chem. Soc.* **2017**, *139*, 3685-3696, DOI 10.1021/jacs.6b11474.
- 11. Lukacs, D.; Nemeth, M.; Szyrwiel, L.; Illes, L.; Pecz, B.; Shen, S. H.; Pap, J. S., Behavior of a Cu-Peptide complex under water oxidation conditions Molecular electrocatalyst or precursor to nanostructured CuO films? *Sol. Energy Mater. Sol. Cells* **2019**, *201*, DOI 10.1016/j.solmat.2019.110079.
- 12. Kaeffer, N.; Morozan, A.; Fize, J.; Martinez, E.; Guetaz, L.; Artero, V., The Dark Side of Molecular Catalysis: Diimine-Dioxime Cobalt Complexes Are Not the Actual Hydrogen

Evolution Electrocatalyst in Acidic Aqueous Solutions. *ACS Catal.* **2016**, *6*, 3727-3737, DOI 10.1021/acscatal.6b00378.

- 13. Artero, V.; Fontecave, M., Solar fuels generation and molecular systems: is it homogeneous or heterogeneous catalysis? *Chem. Soc. Rev.* **2013**, *42*, 2338-2356, DOI 10.1039/c2cs35334b.
- 14. Martin, D. J.; McCarthy, B. D.; Donley, C. L.; Dempsey, J. L., Electrochemical hydrogenation of a homogeneous nickel complex to form a surface adsorbed hydrogen-evolving species. *Chem. Commun.* **2015**, *51*, 5290-5293, DOI 10.1039/c4cc08662g.
- 15. Amatore, C.; Pinson, J.; Saveant, J. M.; Thiebault, A., Trace Crossings in Cyclic Voltammetry and Electrochemic Electrochemical Inducement of Chemical Reactions Aromatic Nucleophilic Substitution. *J. Electroanal. Chem.* **1980**, *107*, 59-74, DOI 10.1016/0368-1874(80)80061-x.
- 16. Rountree, E. S.; McCarthy, B. D.; Eisenhart, T. T.; Dempsey, J. L., Evaluation of Homogeneous Electrocatalysts by Cyclic Voltammetry. *Inorg. Chem.* **2014**, *53*, 9983-10002, DOI 10.1021/ic500658x.
- 17. Martin, D. J.; McCarthy, B. D.; Piro, N. A.; Dempsey, J. L., Synthesis and electrochemical characterization of a tridentate Schiff-base ligated Fe(II) complex. *Polyhedron* **2016**, *114*, 200-204, DOI 10.1016/j.poly.2015.12.003.
- 18. Anxolabehere-Mallart, E.; Costentin, C.; Fournier, M.; Nowak, S.; Robert, M.; Saveant, J. M., Boron-Capped Tris(glyoximato) Cobalt Clathrochelate as a Precursor for the Electrodeposition of Nanoparticles Catalyzing H₂ Evolution in Water. *J. Am. Chem. Soc.* **2012**, *134*, 6104-6107, DOI 10.1021/ja301134e.

- Cronin, S. P.; Al Mamun, A.; Toda, M. J.; Mashuta, M. S.; Losovyj, Y.; Kozlowski, P.
 M.; Buchanan, R. M.; Grapperhaus, C. A., Utilizing Charge Effects and Minimizing
 Intramolecular Proton Rearrangement to Improve the Overpotential of a Thiosemicarbazonato
 Zinc HER Catalyst. *Inorg. Chem.* 2019, 58, 12986-12997, DOI 10.1021/acs.inorgchem.9b01912.
- 20. Cronin, S. P.; Strain, J. M.; Mashuta, M. S.; Spurgeon, J. M.; Buchanan, R. M.; Grapperhaus, C. A., Exploiting Metal-Ligand Cooperativity to Sequester, Activate, and Reduce Atmospheric Carbon Dioxide with a Neutral Zinc Complex. *Inorg. Chem.* **2020**, *59*, 4835-4841, DOI 10.1021/acs.inorgchem.0c00121.
- 21. Phipps, C. A.; Hofsommer, D. T.; Toda, M. J.; Nkurunziza, F.; Shah, B.; Spurgeon, J. M.; Kozlowski, P. M.; Buchanan, R. M.; Grapperhaus, C. A., Ligand-Centered Hydrogen Evolution with Ni(II) and Pd(II)DMTH. *Inorg. Chem.*, DOI 10.1021/acs.inorgchem.2c01326.
- 22. Phipps, C. A.; Hofsommer, D. T.; Zirilli, C. D.; Duff, B. G.; Mashuta, M. S.; Buchanan, R. M.; Grapperhaus, C. A., Metal-Ligand Cooperativity Promotes Reversible Capture of Dilute CO₂ as a Zn(II)-Methylcarbonate. *Inorg. Chem.* **2023**, DOI 10.1021/acs.inorgchem.2c03868.
- 23. Cowley, A. R.; Dilworth, J. R.; Donnelly, P. S.; White, J. M., Copper complexes of thiosemicarbazone-pyridylhydrazine (THYNIC) hybrid ligands: A new versatile potential bifunctional chelator for copper radiopharmaceuticals. *Inorg. Chem.* **2006**, *45*, 496-498, DOI 10.1021/ic0514492.
- 24. Hofsommer, D. T.; Liang, Y.; Uttarwar, S. S.; Gautam, M.; Pishgar, S.; Gulati, S.; Grapperhaus, C. A.; Spurgeon, J. M., The pH and Potential Dependence of Pb-Catalyzed Electrochemical CO₂ Reduction to Methyl Formate in a Dual Methanol/Water Electrolyte. *ChemSusChem* **2022**, *15*, e202102289, 1 8, DOI 10.1002/cssc.202102289.

- 25. Walter, M. G.; Warren, E. L.; McKone, J. R.; Boettcher, S. W.; Mi, Q. X.; Santori, E. A.; Lewis, N. S., Solar Water Splitting Cells. *Chem. Rev.* **2010**, *110*, 6446-6473, DOI 10.1021/cr1002326.
- 26. Trasatti, S.; Petrii, O. A., Real Surface Area Measurements in Electrochemistry. *Pure Appl. Chem.* **1991**, *63*, 711-734, DOI 10.1351/pac199163050711.
- 27. McCrory, C. C. L.; Jung, S. H.; Peters, J. C.; Jaramillo, T. F., Benchmarking Heterogeneous Electrocatalysts for the Oxygen Evolution Reaction. *J. Am. Chem. Soc.* **2013**, *135*, 16977-16987, DOI 10.1021/ja407115p.
- 28. Zhang, T. T.; Zhong, H. X.; Qiu, Y. L.; Li, X. F.; Zhang, H. M., Zn electrode with a layer of nanoparticles for selective electroreduction of CO2 to formate in aqueous solutions. *Journal of Materials Chemistry A* **2016**, *4*, 16670-16676, DOI 10.1039/c6ta07000k.